Multidisciplinary Approach on Characterizing a Mechanochemically Activated Composite of Vinpocetine and Crospovidone

DRITAN HASA,[1] DARIO VOINOVICH,[1] BEATRICE PERISSUTTI,[1] ALOIS BONIFACIO,[2] MARIO GRASSI,[3] ERICA FRANCESCHINIS,[4] STEFANO DALL'ACQUA,[4] MANUELA SPEH,[1,5] JANEZ PLAVEC,[1] SERGIO INVERNIZZI[6]

[1]Department of Pharmaceutical Sciences, University of Trieste, P. le Europa 1, I-34127 Trieste, Italy

[2]Department of Materials and Natural Resources, University of Trieste, P.le Europa 1, I-34127 Trieste, Italy

[3]Department of Chemical Engineering, University of Trieste, P.le Europa 1, I-34127 Trieste, Italy

[4]Department of Pharmaceutical Sciences, University of Padova via F. Marzolo, 5 I-35131 Padova, Italy

[5]Slovenian NMR Center, National Institute of Chemistry, Hajdrihova 19 SI-1001 Ljubljana, Slovenia

[6]Department of Life Sciences, University of Trieste, Via Giorgieri 10, I-34127 Trieste, Italy

Received 12 March 2010; revised 17 June 2010; accepted 24 July 2010

Published online 13 September 2010 in Wiley Online Library (wileyonlinelibrary.com). DOI 10.1002/jps.22331

ABSTRACT: Significant improvement of solubilization kinetics of poorly soluble vinpocetine was obtained through a mechanochemical activation process in presence of micronized crospovidone. Drug-to-polymer weight ratio and milling time variables resulted to have statistically significant impacts on the activation of the product. The complete amorphization was obtained in the coground with the highest crospovidone contents (>80% wt), milled for the longest time (180 min). An *ad hoc* software was then used to calculate the dimensions of the drug crystallites in the samples on the basis of the calorimetric data. The thermal analyses were then accompanied and confirmed by an extensive solid-state characterization, performing X-ray diffraction, Raman imaging/spectroscopy, DRIFT, and SS-NMR spectroscopy, followed by laser diffraction and solubilization kinetics tests. All the analyses agreed on attesting the progressive loosing of crystalline structure of the drug when increasing milling time and amount of polymer in the formulations. This activated status of the drug, which resulted to be homogeneously distributed on the coground sample and stable for at least 1 year, was reflected on favorable solubilization kinetics. The *in vivo* studies on rats revealed that coground systems promoted a fivefold higher oral bioavailability enhancement in comparison to a commercial formulation (Vimpocetin® 5 mg Capsules, Pharma). © 2010 Wiley-Liss, Inc. and the American Pharmacists Association J Pharm Sci 100:915–932, 2011

Keywords: vinpocetine; solid state; mechanical activation; micronized crospovidone; oral absorption; physical characterization; nanocrystals; PXRD; SS-NMR; Raman spectroscopy/imaging

INTRODUCTION

Vinpocetine (VIN) is a semisynthetic derivative of the *Vinca minor L.* alkaloid vincamine.[1] VIN is a poorly water-soluble base-type drug (p*K*a = 7.1).[2] In the pH range between 1.2 and 8.0, VIN solubility enhanced by a reduction in pH and showed an approximately linear relationship between the logarithm of the solubility and pH.[3] It has been shown to improve cerebral circulation and metabolism in the treatment of various types of cerebrovascular circulatory disorders, for example, cerebral infarction, cerebral hemorrhage residual, and cerebral arteries cirrhosis, etc. VIN was introduced in clinical practice in Hungary for the treatment of cognitive

Correspondence to: Dario Voinovich (Telephone: + 39-040-558-3106; Fax. + 39-040-52572; E-mail: vojnovic@units.it)

Journal of Pharmaceutical Sciences, Vol. 100, 915–932 (2011)

disorders and related symptoms.[4] It is mainly used as oral dosage forms, usually in tablets, containing 5 mg of active ingredient, with a daily dosage regimen that can vary between 5 mg_3/day and 20 mg_3/day.[5] However, existing formulations exhibit poor bioavailability (~6.7%)[6–7] and poor absorption.[8] Due to its scarce aqueous solubility and wettability, and extensive metabolism during first pass. An oral formulation with a high degree of oral absorption would, therefore, be highly desirable.

Until now the strategies that have been carried out to enhance VIN oral bioavailability, mainly focused in two directions: first, in preparing liquid and solid self-emulsifying systems, because of its good solubility in oils[9–11] and second, its inclusion in cyclodextrins because of its molecular weight/steric encumbrance and lipophylic nature.[8,12–19]

In this study, an alternative approach has been attempted based on the preparation of binary coground systems with micronized crospovidone (PVP-CL) using an optimized mechanochemical activation process conducted in planetary mill. This approach has been previously successfully applied in the case of another poorly soluble phytochemical, the Sylimarine, from Milk thistle extract.[20,21]

After the preparation of the binary systems in several drug-to-polymer ratios and using different milling times according to an experimental design, the effect of the process and formulation variables on the thermal properties of the product was studied, including the determination of drug crystallite size. Then the systems were analyzed by means of XRD, DRIFT, Raman imaging/spectroscopy, SS-NMR spectroscopy, laser light scattering to ascertain the solid state resulting from mechanochemical activation and to detect possible interactions between components. Finally, the biopharmaceutical performance of the most activated systems was tested *in vitro*, evaluating their solubilization kinetics, and *in vivo,* after oral administration on rats.

MATERIALS AND METHODS

Materials

Vinpocetine was kindly gifted by Linnea SA (Riazzino-Locarno, CH, Switzerland). Micronized crospovidone (PVP-CL®-M) was purchased from BASF/Euphar (Milano, Italy). All other chemicals, of analytical grade, and solvents of high-pressure liquid chromatographic (HPLC) grade, were provided by Carlo Erba (Milan, Italy). Vimpocetin® 5-mg capsules were from Pharma, Hungary and contained the following ingredients: 5 mg of vinpocetine, lactose, and magnesium stearate.

Preparation of Coground Mixtures

Drug and crospovidone were coground in several drug-to-polymer weight ratios according to the experimental plan (Table 1) in a planetary mill Fritsch P5 (Pulverisette, Contardi Fritsch s.r.l., Milan, Italy). The planetary mill was equipped by four agate cylindrical grinding chambers (internal height $H_v = 2.6$ cm, internal radius $R_v = 3.2$ cm, internal volume = 27.5 cm^3) adopting agate balls (diameter 2.2 cm) as grinding media.

Batches of 5 g, previously blend in the suitable proportions (according to the experimental plan below reported) with a stainless steel spatula, were simultaneously coground. The following operative conditions were selected on the basis of a previously published *ad hoc* mathematical model[21]: maximum velocity (10,000 rpm), bowl loading (5 g), number of grinding media (6 agate balls). The grinding procedure was pursued for different milling times, according to the experimental plan reported below, stopping every 15 min for homogeneously mixing the mass with a stainless steel spatula. Two factors, a process variable (milling time-x_1) and a formulation variable (drug to polymer weight ratio-x_2), were selected for investigation. Each factor was considered in different experimental levels: five experimental levels for milling time (60, 90, 120, 150, and 180 min) and six levels for drug-to-polymer weight ratio (1:1; 1:2; 1:3; 1:4; 1:7; and 1:10). The effect of these variables on a solid-state coground characteristic (melting enthalpy-y_1) was evaluated. Preliminary experiments were carried out to select the experimental levels. The experimental plan (shown in Table 1) was designed using NEMRODW program,[22] and the statistical analysis was performed by standard R package.[23] To reduce systematic errors, experiments were completely randomized.

Preparation of Physical Mixtures

For comparison purposes, physical mixtures (PM) were prepared by manually mixing drug and polymer using the same weight ratios as the coground systems.

Differential Scanning Calorimetry (DSC)

Calorimetric analyses were carried out using a differential scanning calorimeter (Mod. TA 4000, equipped with a measuring cell DSC 20 Mettler). The calibration of the instrument was performed with indium, zinc, and lead for the temperature, and with indium for the measurement of the enthalpy. Samples, containing about 2 mg of vinpocetine were placed in pierced aluminum pans and heated at a scanning rate

Table 1. Experimental Matrix-Plan and Observed Response Values.

		Independent Variables				Observed Response
Run	Run Order	X_1	X_2	T (min)	R (wt ratio)	Y [a] (J/g)
1	18	1	1	60	A	45.60
2	1	2	1	90	A	43.70
3	20	3	1	120	A	42.60
4	16	4	1	150	A	38.50
5	6	5	1	180	A	28.90
6	19	1	2	60	B	26.50
7	27	2	2	90	B	23.50
8	17	3	2	120	B	20.40
9	3	4	2	150	B	17.80
10	9	5	2	180	B	13.50
11	7	1	3	60	C	15.10
12	13	2	3	90	C	13.30
13	29	3	3	120	C	9.40
14	5	4	3	150	C	7.10
15	2	5	3	180	C	5.60
16	12	1	4	60	D	9.40
17	30	2	4	90	D	7.50
18	14	3	4	120	D	4.50
19	21	4	4	150	D	2.10
20	10	5	4	180	D	1.80
21	22	1	5	60	E	3.30
22	4	2	5	90	E	2.70
23	11	3	5	120	E	1.60
24	26	4	5	150	E	1.10
25	15	5	5	180	E	0.90
26	23	1	6	60	F	1.10
27	24	2	6	90	F	0.40
28	8	3	6	120	F	0.10
29	28	4	6	150	F	0.10
30	25	5	6	180	F	0.10

Y is the drug melting enthalpy determined by DSC analysis. The independent variables are: T = milling time in min, a factor variable with 5 levels: 60 (1), 90 (2), 120 (3), 150 (4), 180 (5); and R= drug-to-polymer weight ratio, a factor variable with six levels 1:1 (A), 1:2 (B), 1:3 (C), 1:4 (D), 1:7 (E), 1:10 (F).

[a] Y drug melting enthalpy determined by DSC analysis.

of 10°C per min from 30°C to 170°C, under air atmosphere.

Determination of Nanocrystal Fraction and Size Distribution

The estimation of nanocrystal (X_{ncr}) and amorphous (X_a) drug fraction along with with the evaluation of nanocrystal size distribution characterizing coground systems were conducted according to Coceani et al.[24] Briefly, this approach starts from the results of the Brun et al. theory[25] according to which the following relations holds among nanocrystal melting temperature (T_{mr}), specific enthalpy (Δh_{mr}), and radius R^{nc}:

$$\int_{T_{m\infty}}^{T_{mr}} \frac{\Delta h_{mr}}{T}\,dT = -2\left(\frac{\gamma_{sl}}{\rho_s R^{nc}}\right) \quad (1)$$

$$\int_{T_{m\infty}}^{T_{mr}} \frac{\Delta h_{mr}}{T}\,dT = \left(-\frac{2}{R^{nc}}\right)\left[\frac{\gamma_{sl}}{\rho_s} + \gamma_{ls}\left(\frac{1}{\rho_s} - \frac{1}{\rho_1}\right)\right] \quad (2)$$

where $T_{m\infty}$ is the infinite radius crystal melting temperature, γ_{lv} and γ_{sl} are, respectively, liquid drug–vapor and solid drug–liquid drug surface tensions while ρ_s and ρ_l are, respectively, solid and liquid drug density. Equation 1 is based on the hypothesis that the liquid–vapor curvature radius (R^{lv}) is infinite, this happens when the crystal is embedded in a large amount of amorphous drug. Thus, crystal melting occurs inside a large amount of liquid phase. On the contrary, Eq. 2 relies on the hypothesis that R^{lv} is concurrent with R^{nc}, this occurs when many crystals are packed together and, upon melting, each crystal is surrounded by a thin liquid film. Thus, while Eq. 1 applies to low nanocrystal fractions ($X_{ncr} \approx 0$), Eq. 2 holds in the opposite case ($X_{ncr} \approx 1$). In real systems nanocrystals can melt in both the above

mentioned conditions. Accordingly, a way accounting for this situation is to consider the following generalised equation:

$$\int_{T_{m\infty}}^{T_{mr}} \frac{\Delta h_{mr}}{T}\,dT = \left(-\frac{2}{R^{nc}}\right)\left\{X_{ncr}\left[\frac{\gamma_{sl}}{\rho_s} + \gamma_{lv}\left(\frac{1}{\rho_s}-\frac{1}{\rho_l}\right)\right] + (1-X_{ncr})\frac{\gamma_{sl}}{\rho_s}\right\} \quad (3)$$

In order to solve Eq. 3, the approach of Zhang et al.[26] expressing the Δh_{mr} dependence on T_{mr} and R^{nc} was adopted:

$$\Delta h_{mr} = \Delta h_{m\infty} - \frac{3}{R^{nc}}\left(\frac{\gamma_{sv}}{\rho_s}-\frac{\gamma_{lv}}{\rho_l}\right) - \int_{T_{mr}}^{T_{m\infty}} \Delta C_p dT \quad (4)$$

where $\Delta h_{m\infty}$ is the specific melting enthalpy referred to the infinite radius drug crystal, ΔC_p is the difference between the liquid and the solid drug specific heat capacity at constant pressure. As ΔC_p is almost temperature invariant, the third term on the right-hand side of Eq. 4 can be approximated by $\Delta C_p(T_{m\infty} - T_{mr})$ without relevant errors. The determination of $\Delta h_{mr}(R^{nc})$, $T_{mr}(R^{nc})$, and X_{ncr} is achieved by an iterative, numerical, simultaneous solution of Eqs. 3 and 4. Starting from a first guess value for X_{ncr} (typically, $X_{ncr} = 0$) Eqs. 3 and 4 are solved to have a first evaluation of the functions $\Delta h_{mr}(R^{nc})$, $T_{mr}(R^{nc})$. Then, X_{ncr} is recalculated according to:

$$X_{ncr} = \frac{\Delta h_{cg}(T_{mr}, \omega_d)}{\Delta h_{mix}(T_{mco}, \omega_d) - \omega_d(\Delta h_r + \Delta h_T)} \quad (5)$$

where Δh_{cg} is the experimentally determined coground system melting enthalpy referred to the system unit mass (drug plus polymer) and evaluated at T_{mr} (as our carrier, the polymer, is amorphous, Δh_{cg} is only due to drug melting), ω_d is the drug mass fraction characterizing both the physical mixture and the coground system, Δh_{mix} is the melting enthalpy referred to the physical mixture (drug plus polymer) unit mass and evaluated at $T_{m\infty}$ and ω_d while Δh_r and Δh_T are the specific enthalpy corrections (referred to pure drug unit mass) representing, respectively, the nanocrystal melting enthalpy reduction due to nanocrystal radius reduction and melting temperature reduction (see, respectively, the second and third term on the right-hand side of Eq. 4). Δh_r and Δh_T are determined in the simultaneous solution of Eqs. 3 and 4. As our coground systems did not show macrocrystal melting, the amount of amorphous drug fraction (X_a) is simply given by:

$$X_a = 1 - X_{ncr} \quad (6)$$

The determination of nanocrystals size distribution relies on the knowledge of $\Delta h_{mr}(R^{nc})$, $T_{mr}(R^{nc})$, X_{ncr} and on the relation occurring among the volume dV_r occupied by nanocrystals of radius lying in the range $R^{nc} - (R^{nc} + dR^{nc})$ and their specific melting enthalpy (J/kg) Δh_{mr}, melting enthalpy (J) ΔH_{mr} and density ρ_s:

$$\frac{dV_r}{dR^{nc}} = \left(\frac{d\Delta H_{mr}}{dR^{nc}}\right)\left(\frac{1}{\Delta H_{mr}\rho_s}\right) = \left(\frac{Q}{v}\right)\left(\frac{dT_{mr}}{dR^{nc}}\right)\left(\frac{1}{\Delta H_{mr}\rho_s}\right) \quad (7)$$

where t is time, Q is the signal registered by DSC (mW) and v is the DSC heating speed (°C/min). The determination of nanocrystals differential volume distribution [$f(R^{nc})$] can be computed as:

$$f\left(R^{nc}\right) = \frac{dV_r/dR^{nc}}{\int_{R^{nc}_{min}}^{R^{nc}_{max}} (dV_r/dR^{nc})\,dR^{nc}} \quad (8)$$

where R^{nc}_{max} and R^{nc}_{min} represent, respectively, the maximum and minimum value assumed by R^{nc}.

X-Ray Powder Diffraction Studies (XRD)

Solid state of the samples was studied by means of XRD technique using a D500 (Siemens, Munich, Germany) diffractometer with Cu$K\alpha$ radiation (1.5418Å), monochromatized by a secondary flat graphite crystal. The current used was 20 mA and the voltage 40 kV. The scanning angle ranged from 5° to 35° of 2θ, steps were of 0.05° of 2θ, and the counting time was of 5 s/step.

Transmission Electron Microscopy (TEM)

TEM images were taken on Philips EM 208 (Philips, Eindhoven, the Netherlands) at an accelerating voltage of 100 kV.

Diffuse Reflectance Infrared Fourier Transform Spectroscopy (DRIFT)

Diffuse reflectance infrared Fourier transform spectra were obtained on a FT-IR spectrometer (FT-IR Perkin Elmer Spectrum One, Monza, Italy) using the abrasive pad method. The samples (drug, carrier, 1:4 and 1:10 wt coground, and corresponding PM) were previously added to anhydrous KBr (FT-IR grade) in a 1:15 weight ratio (sample to KBr) and gently ground using a pestle, thus avoiding solid transition possibly

induced by extended grinding and yet sample particles are small and evenly dispersed. The scanning range was 450 to 4000 cm^{-1} and the resolution was 4 cm^{-1}, scan number was 8 and scan speed 0.20 cm/s.

Raman Imaging/Spectroscopy

Raman spectra and images were acquired for coground composite, physical mixture, and pure components using an inVia Raman system (Renishaw plc, Wotton-under-Edge, UK), equipped with a 300 mW diode NIR laser emitting at 785 nm (Renishaw) and a ProScanTMII motorized stage (Prior, Cambridge, UK). The laser was focused on the sample (consisting of 300 mg tablets with flat surfaces, prepared from physical and coground mixtures having different drug–polymer ratios, and from pure components) by a 50X objective (0.75 N.A.). To ensure a better sampling for each tablet by taking into account local variations in composition, an area of 84 × 84 μm was mapped with a grid of 2.8 μm (corresponding to 900 spectra per map) for each sample, using the Streamline™ fast imaging configuration and the WiRE 3.1 software (Renishaw), with a total collection time of 13 min/map. Raman maps were then preprocessed (cosmic rays removal and baseline correction) and analyzed with the HyperSpec software package;[27] an average spectrum was calculated for each map, and images depicting the intensity ratio between VIN 1610 cm^{-1} band and the PVP-CL 1668 cm^{-1} band were produced.

Solid-State Nuclear Magnetic Resonance Spectroscopy (SS-NMR)

NMR spectra of solid samples were recorded on Varian Unity Inova 300 MHz NMR spectrometer equipped with 5 mm Magic Angle Probe and Varian NMR system 600 MHz NMR spectrometer equipped with 3.2 mm NB double resonance HX MAS solids probe. Larmor frequencies of protons and carbon nuclei were 302.98 MHz and 76.19 MHz at 300 MHz NMR spectrometer, respectively and 599.77 MHz for protons at 600 MHz NMR spectrometer. The proton and ^{13}C CP/MAS NMR spectra were externally referenced using adamantine or hexamethylbenzene, respectively. All samples were spun at the magic angle with 5 kHz spinning frequency during ^{13}C measurements at 300 MHz NMR spectrometer and 20 kHz during ^{1}H measurements at 600 MHz NMR spectrometer. The proton spectra were acquired using spin echo sequence. Repetition delay in all experiments was 5 s. The number of scans was 16. The pulse sequence used for acquiring the ^{13}C CP/MAS spectra was a standard cross-polarization MAS pulse sequence with high-power proton decoupling during acquisition. Repetition delay in all experiments was 3 s and the number of scans was between 8000 and 27,000 depending on the signal-to-noise ratio.

Particle Size Measurements

Particle size measurements of the coground were determined using a laser light scattering technique (Malvern Particle Size Analyzer Model No. 2000, Malvern, UK). Before analysis, about 10 mg of composite was dispersed by sonication in 100 mL of water.

Release Kinetics

Release tests, performed in triplicate, were led in 150 cm^3 of 0.2 M KH_2PO_4/0.2 M NaOH (pH 7.4) at 37°C. At this pH value, the solubility was 1.6 mg/L. A suitable amount of pure drug or binary system corresponding to 5 mg of active ingredient was added to the release environment at time zero. Uniformity conditions were ensured by an impeller (rotational speed 200 rpm). The use of a fiber optic apparatus (HELLMA, Milano, Italy), connected to a spectrophotometer (ZEISS, Germany, wavelength 270.19 nm), allowed the determination of vinpocetine concentration without perturbing the release environment (each release test lasted 180 min). Moreover, this methodology allowed to easily overcome the problem connected to drug concentration measurement in presence of a dispersion of solid particles. Indeed, while the maximum vinpocetine absorption occurred at 270.19 nm, the scattering effect due to polymeric particles uniformly occurred at every wavelength. Accordingly, the real absorbance related to vinpocetine concentration was the difference between the absorbance measured at 270.19 nm and that measured at 500.49 nm (at 500.49 nm vinpocetine did not absorb). Non-sink conditions were attained in release environment. Results were the average of three replicates and standard deviations did not exceed 5%.

In Vivo Absorption Studies

Experiments on animals complied with the Italian D.L. n. 116 of 27 January 1992 and associated guidelines in the European Communities Council Directive of 24 November 1986 (86/609 ECC).

Animals used were male Sprague-Dawley rats (450 g weight) and were supplied by Centro Servizi Polivalenti di Ateneo (University of Trieste, Trieste, Italy). Rats, with free access to water, were fasted overnight. Each experimental formulation was administered to four rats by gastric gavage as 2 mL of aqueous suspensions (corresponding to a dose 11 mg/kg of vinpocetine).

Blood samples (600 μL) were collected using the "cannulated" tail artery method[28] in heparinized tubes at 30, 60, 90, 120, 180, and 360 min after administration. Blood samples were added to 66 μL of a 40 mM tetrasodium EDTA solution, centrifuged at 166 g for 10 min and plasma was separated and immediately frozen at −20°C, and stored at this temperature till the analysis.

Assays of Vinpocetine in Powder and Plasma Samples

HPLC Sample Preparations

For the determination of the drug content in physical mixtures, coground systems, and commercial sample the following procedure was followed: a suitable amount of powdered sample was accurately weighted and transferred to a 100 mL volumetric flask and diluted with acetonitrile. The mixture was sonicated for 10 min and then filtered through a syringe filter (RC 0.45 μm, Phenomenex, Castel Maggiore, Bologna) to remove any particle. The first 5 μL of the filtrates was discarded and the subsequent filtrates were collected. Then, an appropriate amount of the filtrate was diluted with acetonitrile and assayed by a validated HPLC with mass spectrometry (MS) detection method,[29] details are described later.

As for the determination of vinpocetine in plasma samples, the following procedure was adopted. Briefly, 600 μL methanol was added to 200 μL plasma, and the mixture was vortexed for 10 min. After centrifugation (1845 g for 6 min), 5 μL of the organic solution was injected. The vinpocetine determination was carried out using the same HPLC-MS method.

HPLC Analysis

The HPLC system consisted of a Varian LC212 with a 500-MS IT mass detector. The chromatographic separation was conducted at room temperature, using a Varian C 18 Polaris column (3 μm, 2.0 × 50 mm). The mobile phase was composed of water with 0.1% formic acid (solvent A) and acetonitrile (solvent B). Isocratic conditions were used with A 57: B 43, total run time was 3 min. The flow rate was 200 μL/min.

MS conditions: ESI (positive mode), needle voltage 5350 V, drying gas temperature was 400°C, capillary voltage was set to 100 V and RF loading was set to 100%, nebulizer gas pressure was 25 psi; drying gas pressure was 15 psi. The detector was set to monitor $m/z = 290–390$.

The calibration curve for vinpocetine ranged from 14.5 to 142.40 ng/mL (plasma). The limit of quantification was 2 ng/mL. The precision and accuracy were under 3% for all calibration points.

Pharmacokinetic Analysis

Pharmacokinetic parameters of coground, physical mixtures, and commercial tablets were calculated on the plasma curves. The area under the plasma concentration–time curve extrapolated to the last sampling time at which a quantifiable concentration is found (AUC_{last}) was calculated using the log-linear trapezoidal method. Time and value of maximum concentration (t_{max} and C_{max}, respectively) were reported as observed. The relative bioavailability after oral administration (F_{rel}) was calculated in Eq. 1:

$$F_{rel} = \frac{AUC_{(COGorPM)}}{AUC_{(Commercial)}} \quad (9)$$

Pharmacokinetic analysis was performed using WinNonlin Version 2.1 (Pharsight Corporation, Mountain View, California) software.

RESULTS AND DISCUSSION

As discussed earlier, the aim of the work was to employ the mechanochemical activation process for enhancing the solubility of vinpocetine, thus possibly improving its oral bioavailability. In this case, the phytochemical drug was coground with a cross-linked polymer, PVP-CL, in different drug-to-polymer weight ratios and using different milling times, according to an experimental plan (Table 1), to check the effect of these formulation and process variables on the characteristics of the coground product. The process was conducted in a Fritsch P5 planetary mill that is particularly suitable for its lab scale for performing a study of screening among variables. In this apparatus, the solid-state activation is mainly achieved by the creation of shearing interactions, as a result of the rolling of ball elements on the wall of the grinding container. As the response of the experimental plan, the drug melting enthalpy in the coground system (determined by DSC analysis) was considered. It is in fact well known that the melting enthalpy is related to crystallinity of the sample, and hence this parameter can be very useful to check possible structural changes in the product evidence of the "activation" of the product. As a first step, it is therefore very important to select the optimal process and formulation conditions for reducing drug melting enthalpy through an appropriate experimental design.

Because single runs were carried out, a full two-way ANOVA model with interaction was not adoptable. In fact, the number of observations is equal to the number of parameters. Actually, the parameters could be estimated, but no further inference would be possible. In this case, the literature suggests the graphical approach to evidence the interaction between independent variables.[30]

As it can be observed from Figure 1, the drug melting enthalpy Y decreased with increased milling time T, and slightly faster for higher drug-to-polymer weight ratio R. In both cases, the curves were not perfectly parallel.

For the purposes of this study and for the sake of simplicity, no interactions were assumed. The following model without interaction was thereby fitted:

$$Y_{ij} = \mu + \alpha_i + \beta_j + \varepsilon_{ij} \quad (10)$$

 DOI 10.1002/jps

Table 2. Summary of the Two-Way ANOVA model ($R^2 = 97.82\%$, Adjusted $R^2 = 96.84\%$)

	Estimate	Std. Error	t-Value	Pr (> |t|)
(Intercept)	43.753	1.481	29.545	$< 2 \times^{-16}$***
$T = 90$	−1.650	1.481	−1.114	0.278416
$T = 120$	−3.733	1.481	−2.521	0.020303*
$T = 150$	−5.717	1.481	−3.860	0.000975***
$T = 180$	−8.367	1.481	−5.650	1.57×10^{-5}***
R = B (1:2)	−19.520	1.622	−12.033	1.30×10^{-10}***
R = C (1:3)	−29.760	1.622	−18.345	5.58×10^{-14}***
R = D (1:4)	−34.800	1.622	−21.451	2.82×10^{-15}***
R = E (1:7)	−37.940	1.622	−23.387	5.34×10^{-16}***
R = F (1:10)	−39.500	1.622	−24.349	2.45×10^{-16}***

As basic levels (response = intercept) of the independent variables $\boldsymbol{T} = 60$ min, and $\boldsymbol{R} = 1{:}1$ (level A) are assumed. By applying the Shapiro-Wilk normality test for the residuals, ε has p-value = 40.22% (thus normality cannot be rejected).

Significance codes (α): ***$p = 0.001$, *$p = 0.05$.

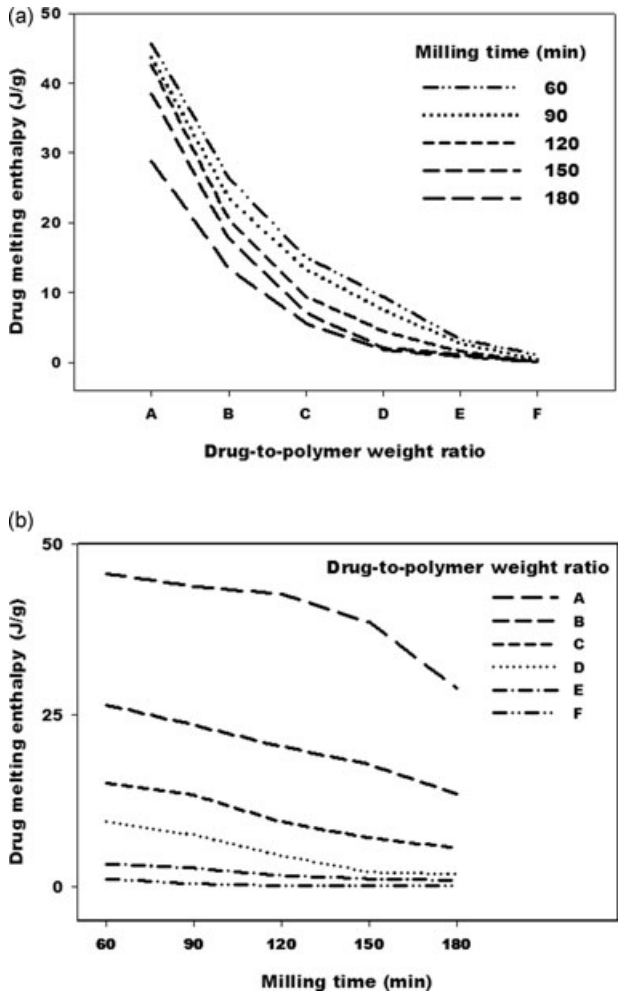

Figure 1. Interaction plots of the experimental variable with the 2 independent variables considered at different levels: milling time T (a) and drug-to-polymer weight ratio (b).

where μ is the ground state of Y, and α_i and β_j are the effect of milling time T and drug-to-polymer weight ratio R, respectively. The results obtained using the standard R package (R Development Core Team)[23] is listed in Table 2.

From the overall analysis of Figure 1 and Table 2, it appears that the most significant changes of drug solid state are obtained with longest milling time (150 and 180 min) and with all the performed variations of coground composition.

This behavior is quite reasonable. In fact, vinpocetine can be easily trapped into the amorphous physically cross-linked polymer as the polymer amount increases. Once embedded, it would be probably stabilized in the metastable amorphous or nanocrystalline form. On the other hand, the time factor is also important. As the milling time increases, a higher quantity of mechanical energy due to the tangential mechanical strain of the planetary mill is transferred to the material, thus inducing more pronounced structural changes in the sample.

For brevity, the systems prepared with the longest milling time (180 min) will be selected for further considerations.

Looking at the DSC traces of the coground systems (Fig. 2), in comparison to native drug and simple physical mixtures, the following points can be considered.

The pure drug showed an endothermal event at 149.6°C (Fig. 2a), while the amorphous polymer exhibits only an endothermic hump due to its dehydration upon heating (Fig. 2b). The physical mixtures prepared in different drug-to-polymer ratios showed a complete absence of interactions among components. In fact, the thermograms (Fig. 2, traces from C to H) are the sum of the thermal events of the drug and the polymer, whereas the drug melting enthalpy is proportional to the drug content in the systems. The DSC traces of the systems coground in different drug-to-polymer weight ratios for the same milling time (180 min) are compared in Figure 2b. In this image, the vinpocetine melting peak noticeably shifted to lower temperatures when increasing the amount of PVP-CL. Furthermore, the drug melting event is characterized

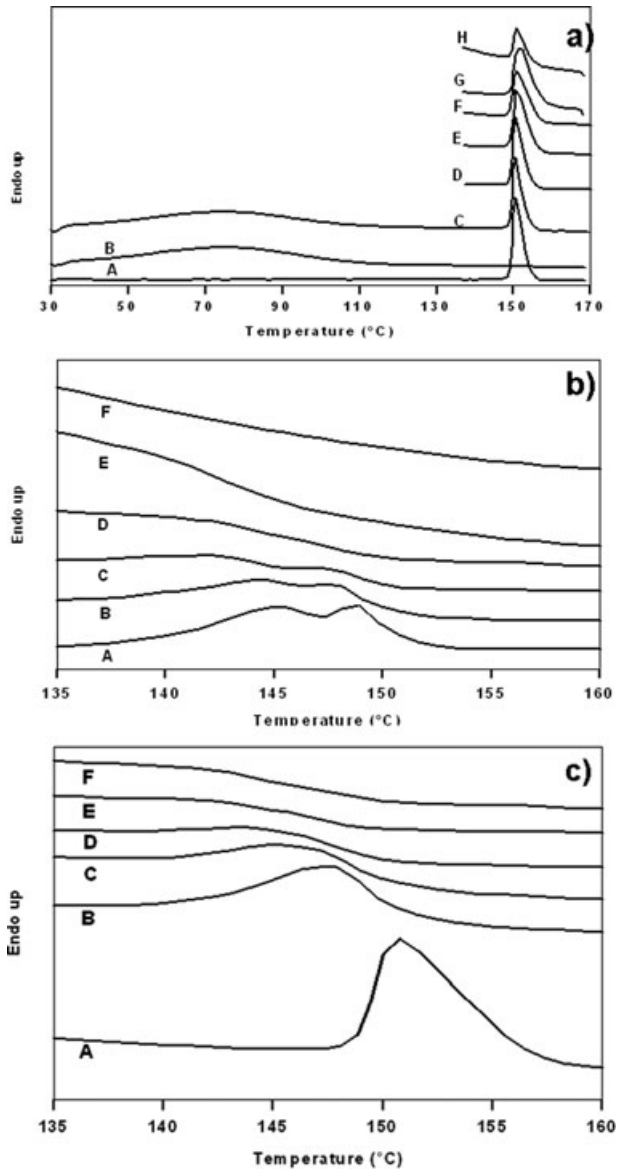

Figure 2. a) DSC traces of pure vinpocetine (A), PVP-CL (B) and 1:1 (C), 1:2 (D), 1:3 (E), 1:4 (F), 1:7 (G), 1:10 (H) wt physical mixtures; b) DSC traces of 1:1 (A), 1:2 (B), 1:3 (C), 1:4 (D), 1:7 (E), 1:10 (F) systems coground for 180 min; c) DSC traces of 1:4 wt physical mixture (A) and 1:4 wt systems coground for 60 (B), 90 (C), 120 (D), 150 (E), 180 (F) minutes.

by a progressive broadening of the endothermal and by a progressive reduction of relative enthalpy with increased proportions of carrier. In addition, the effect of milling time on the drug melting event can be seen in Fig. 2c (for the sake of brevity only the 1:4 weight ratio is reported) where a progressive reduction of drug melting enthalpy and drug melting peak can be observed with increasing the milling time. The decreasing and the broadening of the melting peak indicate the formation of nanocrystalline structure, whereas the decreasing of melting enthalpy indicates

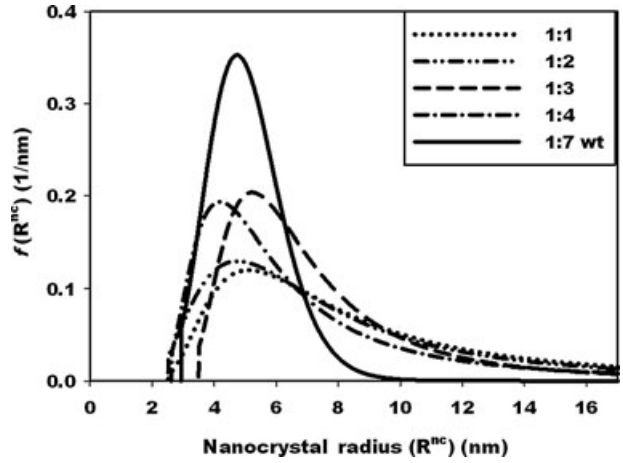

Figure 3. Differential distribution of the nanocrystal radius in the coground systems depending on their composition. Due to its total amorphouness (see table 3), the plot of the 1:10 wt coground system is not reported.

the presence of amorphous vinpocetine.[31] Hence, it would be interesting on the basis of the DSC features to ascertain not only the degree of crystallinity reached by each coground sample, but also the size of drug crystallites and their distribution in each sample.

These details were obtained by DSC data analysis according to the home-made MELTINGDSC software whose principles were briefly presented in the "determination of nanocrystal fraction and size distribution" section. The resulting percentages of amorphous and/or nanocrystalline drug in the coground systems are reported in Table 3, while the differential distribution of the crystal radius in the composites depending on their composition is depicted in Figure 3.

In the coground systems treated for 180 min, the percentage of amorphous drug increased as the polymer content augmented while that of nanocrystalline drug simultaneously diminished. Furthermore, the drug melting point and the drug melting enthalpy progressively diminished as the polymer content increased. These thermal phenomena were thus evidence of the progressive destructuration of crystalline lattice of vinpocetine and its progressive conversion with increased polymer content. The complete destructuration of drug crystal lattice is achieved with the 1:10 wt system, appearing completely amorphous ($X_a = 99.90\%$).

As for the differential distribution of the crystal radius in the composites in the various compositions, from Figure 3, it appears that while peak frequency is almost constant (around 5 nm), size distribution is progressively narrowing as polymer content increased. This underlines the importance played by polymer content in getting a homogeneous system (from the nanocrystal size distribution point of view).

 DOI 10.1002/jps

Table 3. Different Nanocrystalline and Amorphous Percent Fractions in the Systems Coground for 180 min

Drug-to-Polymer Weight Ratio	T_{mr} (°C)	ω_d	Δh_{mix} ($T_{m\infty}$)	Δh_{mix} (T_{mr})	Δh_{cg}	X_{ncr} (%)	X_a (%)
1:1	148.4	0.5	46.56	45.83	27.70	60.50	39.50
1.2	144.4	0.33	30.32	29.10	13.81	47.50	52.50
1:3	142.5	0.25	22.40	21.15	6.38	30.20	69.80
1:4	142.2	0.2	17.98	17.04	2.73	16.00	84.00
1:7	139.9	0.125	11.05	10.28	0.91	8.80	91.20
1:10	133.5	0.091	7.67	6.74	0.01	0.10	99.90

T_{mr}, nanocrystal melting temperature determined by DSC analysis; ω_d, drug mass fraction; $\Delta h_{mix}(T_{m\infty})$, melting enthalpy referred to the physical mixture unit mass and evaluated at $T_{m\infty}$(149.6 °C) and ω_d; $\Delta h_{mix}(T_{mr})$, melting enthalpy referred to the physical mixture evaluated at T_{mr} and ω_d; Δh_{cg}, experimentally determined coground system melting enthalpy evaluated at T_{mr}; X_{ncr}(%), nanocrystalline drug percentage; X_a (%), amorphous drug percentage.

Probably, this behavior can be explained by the polymer stabilization action that should be proportional to polymer content.

To verify the success of the research objectives, so to enhance the oral vinpocetine bioavailability, the subsequent step involved in the evaluation of the *in vitro* dissolution performances of the coground systems using the solubilization kinetics method in comparison to the physical mixtures and the pure vinpocetine (Fig. 4). In particular, in the light of the aforementioned statistical analysis, the systems treated for the longest time and having six different types of polymer content were analyzed.

The simple physical mixtures, independent of the polymer content, displayed dissolution profiles not significantly different and almost super-imposable to that of pure drug (see Fig. 4, where for brevity, only 1:10 wt PM is reported). Conversely, the activated state of the coground systems, demonstrated by previous thermal analyses, was reflected in a remarkable improvement of dissolution performance in comparison to the physical mixtures and the pure drug. In fact, less energy is required to dissolve the "activated" drug (nanocrystalline and/or amorphous drug) with respect to the original stable crystalline phase.

Among different coground systems, the best performances, both in terms of rate and extent of dissolution, can be achieved from the systems containing more than 80% wt of PVP-CL. These mechanochemically treated systems after 180 min showed an increase in the solubilized amount ranging from 124- to 190-fold, depending on the composition, in absence of supersaturation phenomena. Amongst the three best performing coground systems, the 1:4 and 1:10 wt, representing the compositions at the boundaries, were selected for further characterizations.

In particular, the following analyses were performed to complete the solid-state investigation, such as X-ray diffraction, DRIFT, Raman imaging/spectroscopy, and SS-NMR analysis.

Figure 5 reports the diffractograms of the 1:4 and 1:10 wt coground systems compared to the PM and the raw materials. Besides the complete lack of peaks and the halo pattern, typical of amorphous materials, detected in the pattern of PVP-CL (Fig. 5f), the drug

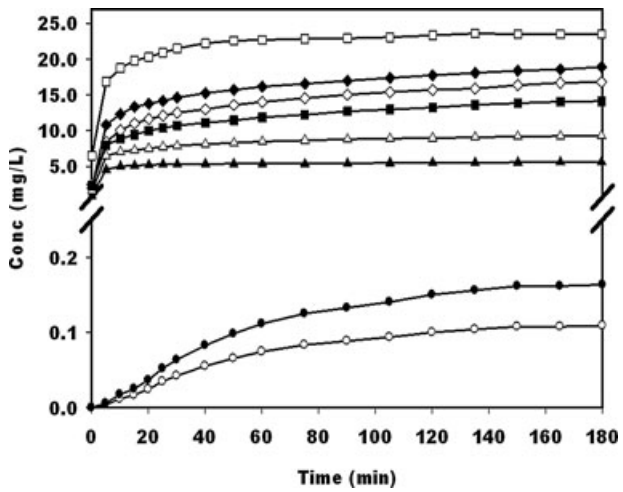

Figure 4. In vitro solubilization kinetics in pH 7.4 of pure vinpocetine (○), compared to the 1:10 wt PM (●) and the coground systems with different wt compositions (1:1 ▲, 1:2 △, 1:3 ■, 1:4 ◊, 1:7 ◇, 1:10 □).

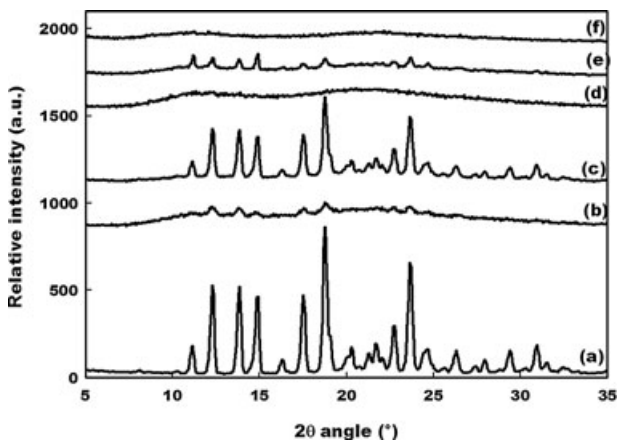

Figure 5. XRD pattern of pure vinpocetine (a), 1:4 wt coground for 180 min (b), 1:4 wt PM (c), 1:10 wt coground for 180 min (d), 1:10 wt PM (e) and PVP-CL (f).

shows intense reflections (Fig. 5a) indicating its crystalline nature. In particular, the diffractogram is very similar to that previously reported for vinpocetine by Ribeiro et al.[16] : the major peaks are appearing in the range between 10° and 25° of 2θ.

Observing the XRD patterns of the 1:4 active ingredient to polymer weight ratios binary system coground for 3 h, the major drug reflections are still detectable (Fig. 5b). When they are compared with the corresponding PM (Fig. 5c), a dramatic reduction of their intensity, a slight broadening of the reflections, and a remarkable underneath scattering phenomenon can be noticed. These facts are evidence of the partial conversion of the original crystal lattice into an amorphous and/or nanocrystalline phase, in agreement to previous thermal analyses. Interestingly, the XRD pattern 1:4 wt coground (Fig. 5b) revealed that cogrinding did not result in the formation of polymorphs as the peaks are exactly those related to pure VIN (see Fig. 5a).

XRD analysis also testified that in the case of the coground system 1:10 VIN:PVP-CL wt, the complete amorphysation was reached (Fig. 5d). In this pattern, two large humps can be recognized, resulting from the polymer that shows its peaks at about 12° and 22° 2θ (see Fig. 5f). On the contrary, no peaks referred to VIN can be detected (see Fig. 5a). As in the XRD pattern of the 1:10 wt PM (Fig. 5e) the VIN characteristics peaks emerged, VIN peaks disappearing in the XRD pattern of the coground system 1:10 VIN:PVP-CL wt cannot be attributed to the simple attenuation of the drug signals due to the high amount of crospovidone.

Furthermore, the same coground samples (1:4 and 1:10 wt) were assayed by TEM analysis. The 1:4 wt coground sample (Fig. 6a) appeared as spherical structures formed by the polymer embedding the active ingredient. In particular, the cross-linked network of PVP-CL can be clearly seen together with the nanocrystalline drug formations (dark structures) having dimensions compatible with those previously calculated by the MELTINGDSC program. Once again in agreement with previous characterizations, the 1:10 wt coground samples appeared completely amorphous (Fig. 6b). It can be concluded that TEM pictures provided direct evidence of the existence of nanocrystalline phase only in the case of 1:4 wt composite.

The characterization was then pursued by means of DRIFT technique, because vibrational changes can serve as probes of intermolecular interactions in solid materials. For brevity, in Figure 7 the region of 1800–500 cm^{-1} of DRIFT spectra has been reported, comparing the features of 1:4 and 1:10 wt coground system with corresponding PMs and starting materials. The major difference between PMs and coground systems can be noticed in the VIN C=O stretching band (originally at 1713 cm^{-1}). This seems to indicate that the aforementioned disruption of the crystalline lattice mainly leads to changes in the conformation or orientation of this group.

More Information from Raman Spectroscopy

Raman spectra collected from tablets prepared with physical and coground mixtures of different VIN/PVP-CL weight ratios show bands of both drug and polymer (Fig. 8).

Spectra of physical mixtures are an exact superposition of the two components, all bands being unaffected in frequency or relative intensity, suggesting little or no interaction between VIN and PVP-CL.

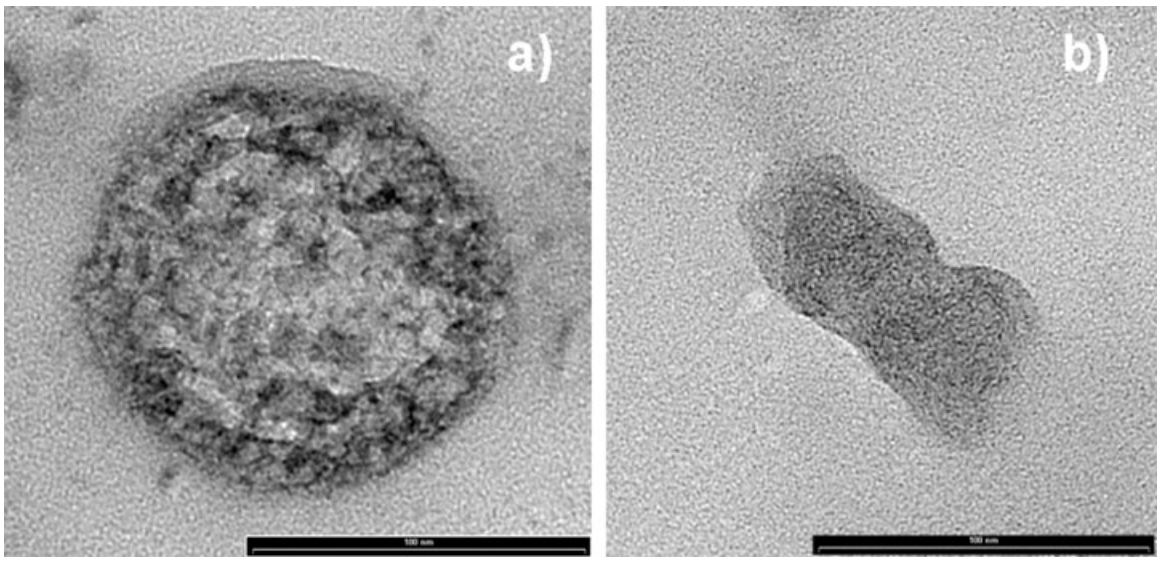

Figure 6. TEM image of samples coground for 180 min in the 1:4 wt (a) and 1:10 wt (b) drug-topolymer ratios.

 DOI 10.1002/jps

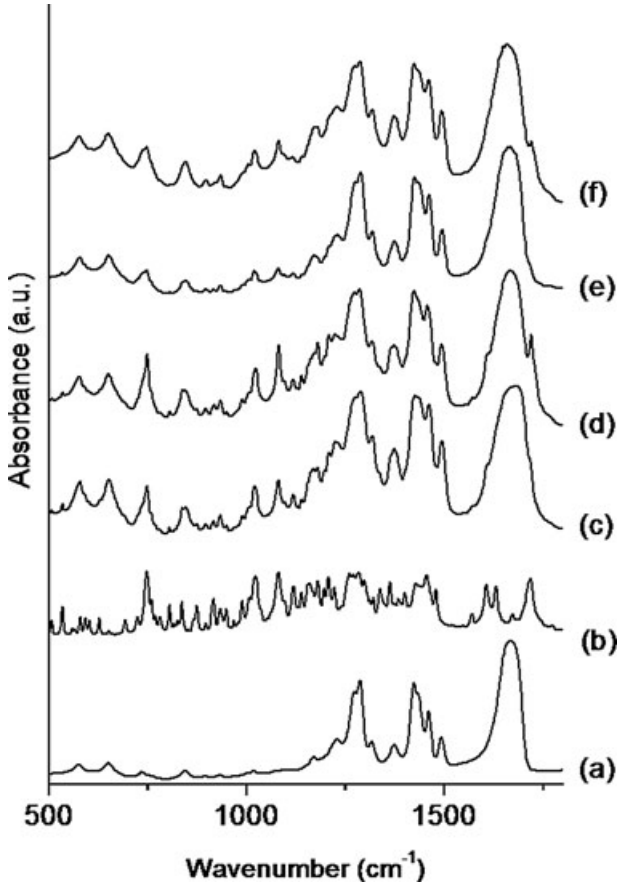

Figure 7. DRIFT spectra of (a) PVP-CL, (b) VIN, (c) 1:4 wt PM, (d) 1:4 wt COG, (e) 1:10 wt PM, (f) 1:10 wt COG (1800-500 cm^{-1} range).

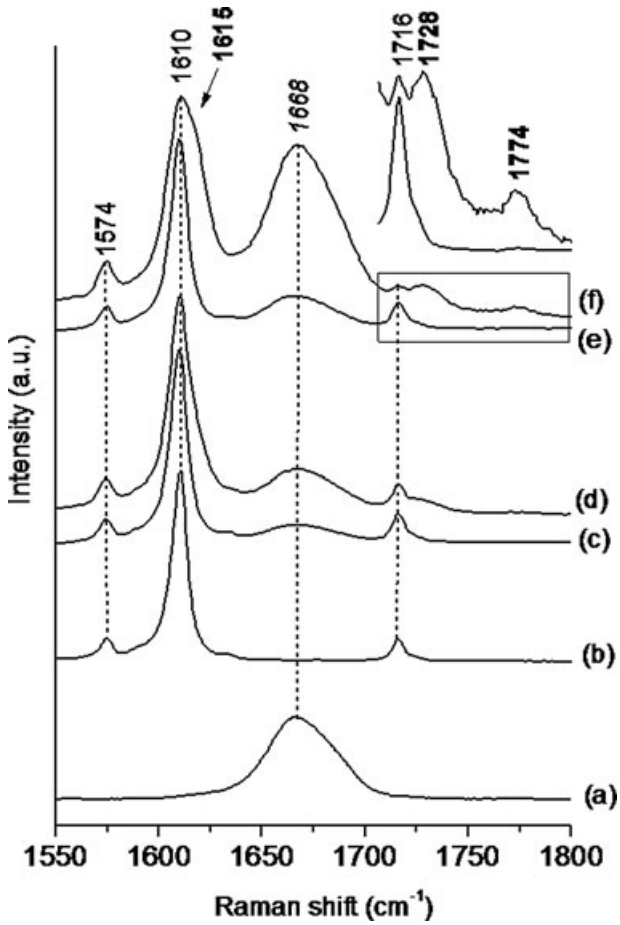

Figure 8. 1550-1800 cm^{-1} regions of Raman spectra of tablets of (a) PVP-CL, (b) VIN, (c) 1:4 wt PM (d) and coground, (e) 1:10 wt PM and coground (f); (c) – (f) are averages obtained from Raman maps of 84×84 Dm containing 900 spectra each. The 1700-1800 cm^{-1} spectral region of (e) and (f) is shown on the upper right with rescaled intensity. Bands attributed to VIN which are present only in the coground mixtures are labeled in bold, PVP-CL C=O stretching is labeled in italic. Excitation wavelength is 785 nm.

Also in coground mixtures, most bands are unshifted with respect to the pure components, with the exception of some bands in the 1550–1800 cm^{-1} region, which shows some spectral changes. In the coground mixtures the VIN band at 1610 cm^{-1}, attributed to an aromatic C=C stretching, broadens toward higher frequencies. This broadening is present in all coground samples and increases with the relative ratio of polymer, being most pronounced in the spectrum of the 1:10 ratio mixture, where a distinct shoulder at 1615 cm^{-1} can be observed (Fig. 8f). Increasing the ratio of polymer in the coground samples also causes the VIN band at 1716, assigned to the C=O stretching, to shift at 1728 cm^{-1}, together with the appearance of a band at 1774 cm^{-1}, which is clearly observed in the 1:10 mixture. These spectral changes are present exclusively in the coground mixtures, and suggest an interaction between the drug and the polymer, which is absent in the physical mixtures. The exact nature of this interaction is difficult to assess, although some hypotheses can be drawn. The absence of any shift in the PVP-CL C=O stretching band at 1668 cm^{-1} indicates that hydrogen bonding plays little or no role in the polymer—drug interaction.[32] This is not surprising because both molecules in their neutral forms contain H-bond acceptors but no donors.

However, it is noticeable that the shift of the VIN C=O stretching band indicates an alteration of the carbonyl environment with respect to the pure substance or to the drug in the physical mixture, similarly to what was detected in the FT-IR spectra.

Most importantly, the shift of the VIN aromatic C=C stretching band at 1610 suggests a perturbation of the aromatic moiety of VIN, possibly indicating a hydrophobic interaction between the drug and the polymer, or a polymer-induced change of drug—drug hydrophobic interactions. A similar effect has been reported in the case of the aromatic C=C stretching band of ibuprofen in its mixtures with PVP-CL.[33] Despite the absence of a general band broadening,

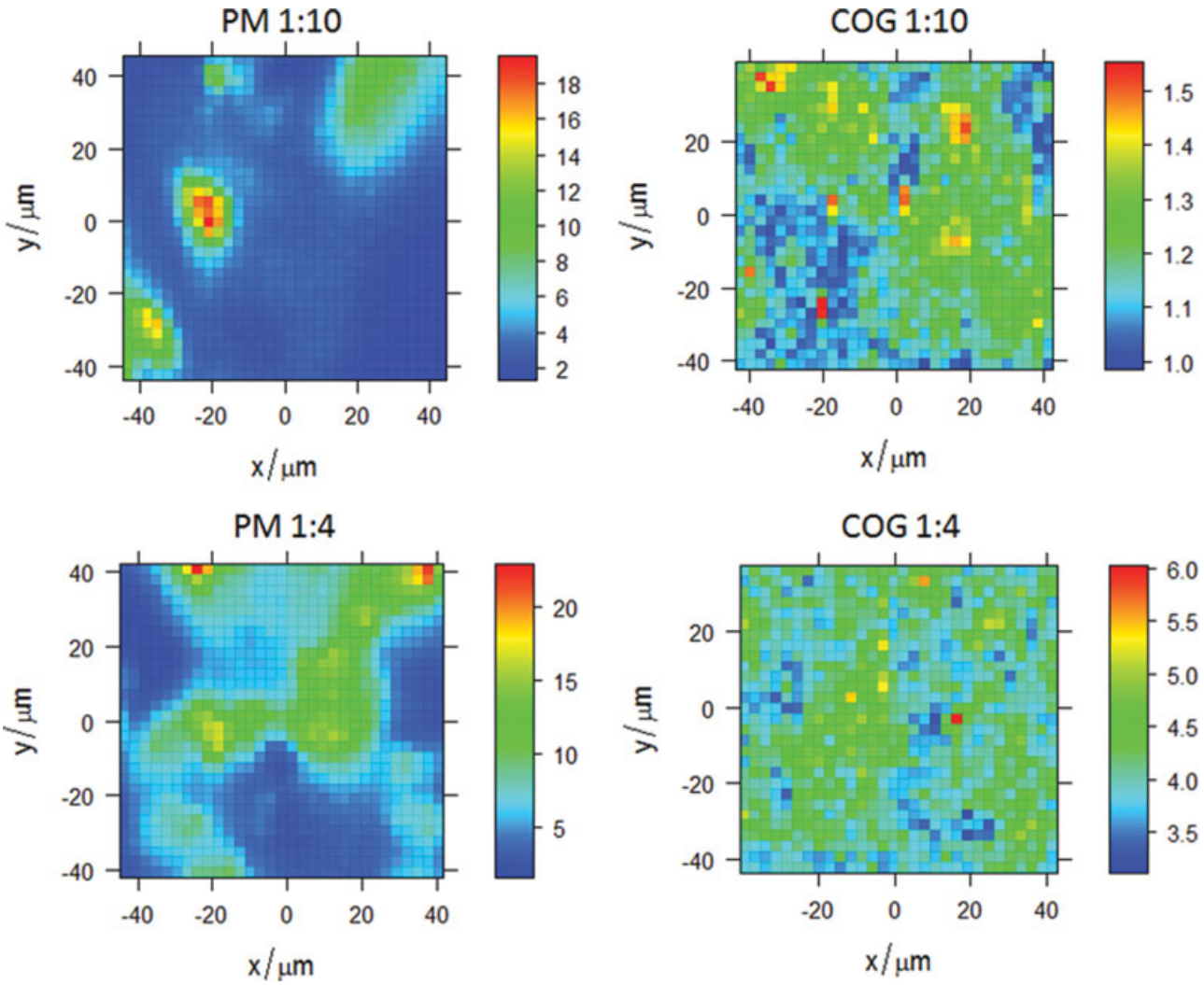

Figure 9. Images depicting the density distribution of VIN in tablets consisting of physical mixtures (PM, left) and coground (COG, right) of VIN and PVP-CL in 1:10 (above) and 1:4 (below) ratios. Images are constructed from Raman maps upon imaging the intensity ratio between the 1610 cm^{-1} band (C=C stretching) of VIN and the 1668 cm^{-1} band (C=O stretching) of PVP-CL.

which could be justified by the rigid VIN molecular structure, these changes in the Raman spectra of the coground mixtures could be interpreted as the disruption of the drug crystals by the cogrinding process, which induces an alteration in the C=O and C=C stretching of VIN.

Raman spectroscopy has also been used to evaluate the effect of the cogrinding process on the spatial heterogeneity of the mixtures at microscopic level. The analysis of the Raman maps of tablets prepared from physical and coground mixtures having different drug–polymer ratios showed that VIN is distrubuted much more homogenously in the coground samples than in the physical mixtures (Fig. 9).

Solid-state NMR has been then used to further study the solid state of the samples and to understand the nature of interactions between components.

The ^{13}C CP/MAS NMR spectra of solid samples of the pure materials, VIN and PVP-CL, are reported in Figures 10a and 10b, respectively. Figure 10a shows a spectrum of VIN with narrow signals indicating the crystalline nature of the sample, while Figure 10b shows the spectrum of polymer PVP-CL having broad signals as typical of amorphous substances. NMR spectra of physical mixtures of the aforementioned pure compounds in 1:4 and 1:10 drug-to-polymer weight ratios are shown in Figures 10c and 10d, respectively. Weight ratio of the pure compounds in physical mixtures can be nicely seen, for instance, from the comparison of the signal intensities in carbonyl region of NMR spectra.

To establish crystalline or amorphous nature of investigated compounds, the signals corresponding to carbonyl groups has been enlarged (Fig. 11) In this

 DOI 10.1002/jps

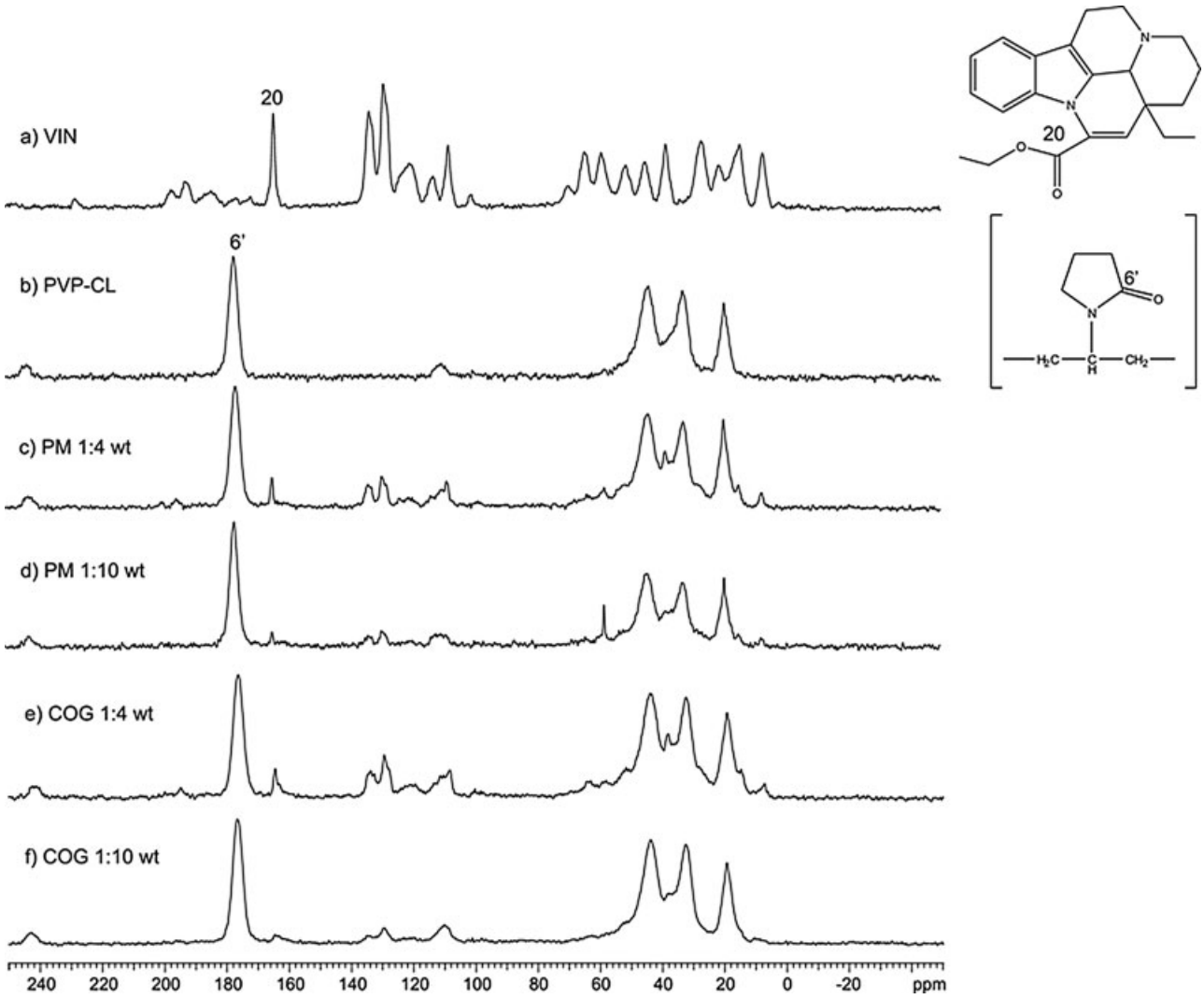

Figure 10. ^{13}C CP/MAS NMR spectra of a) VIN, b) polymer PVP-CL, c) physical mixture 1:4 wt, d) physical mixture 1:10 wt, e) coground mixture 1:4 wt and f) coground mixture 1:10 wt. In a) and b) carbonyl atoms are marked.

part of the spectra, it can be nicely seen that the signals corresponding to the C20 atom of VIN inside physical mixtures of both studied weight ratios are still narrow (Figs. 11a and 11b). This observation suggests that the nature of the compound in the physical mixture did not change with respect to the original compound.

In the case of coground mixture at ratio of polymer PVP-CL and VIN molecules of 1:4, a narrow signal corresponding to the C20 carbon atom of VIN molecule can be still observed (Fig. 11c). According to the feature of VIN C=O group in the Raman spectra, the observed signal in this case has a broad shoulder on the right-hand side, suggesting that VIN molecules are partially in an amorphous state. It means that different types of VIN molecules are present in this sample, both crystalline and amorphous forms. When increasing the amount of PVP-CL in the coground sample (1:10 wt system), only broad signals have been observed for carbonyl C20 atom of VIN (Fig. 11d). Broad nature of the signals indicates the complete transformation of VIN molecules in an amorphous form at this weight ratio. These findings are in complete agreement with previous DSC and XRD results.

^{1}H NMR spectra of the parent compounds VIN and PVP-CL, as well as physical and coground mixtures (Fig. 12), have also been recorded with the purpose of ascertaining further the absence of hydrogen bonding in the samples.

In proton spectra, signals belonging to protons involved in hydrogen bonds were not observed, in accordance with the aforementioned Raman data. A spectrum of polymer PVP-CL shows three sharp signals with chemical shifts of 4.19, 3.65, and 1.23 ppm indicating the presence of water molecules in different environments inside the solid sample

Table 4. Vinpocetine Pharmacokinetic Parameters After Oral Administration in Rats of the Coground Systems, Corresponding Physical Mixtures and Commercial Reference (mean ± S.D., $n = 4$).

Formulations	C_{max} (ng/mL) ±S.D.	t_{max} (min)	$AUC_{(last)}$ ng/(h mL)	F_{rel}
Coground 1:10 wt	101.0 ± 28.4	30	141.4 ± 36.6	1.8
PM 1:10 wt	61.3 ± 4.5	30	91.5 ± 12.9	1.2
Coground 1:4 wt	199.2 ± 39.0	30	397.7 ± 62.5	5.1
PM 1:4 wt	57.9 ± 4.8	30	84.5 ± 11.8	1.1
Vimpocetin® 5 mg	33.0 ± 5.0	120	78.5 ± 14.7	1

(Fig. 12b). Signals with higher chemical shift (4.19, 3.65) most likely belong to clusters of pure water somewhere on the surface of the molecule, while the signal at $\delta = 1.23$ ppm corresponds to monomeric water.

To ascertain the nature of these three sharp signals and whether they indeed belong to the water molecules, the sample has been dried (at 40°C for 24 h under vacuum). The proton NMR spectrum of dried PVP-CL sample (data not shown), having at the thermogravimetrical analysis (TA Instruments, New Castle, Delaware) a residual water content <1%, did no longer exhibit the above-mentioned sharp signals.

In the case of VIN, we did not observe any sharp signals but only two large humps, originated from signals much lower than those belonging to PVP-CL protons (Fig. 12a).

Spectra of physical mixtures (Figs. 12c and 12d) and coground mixtures (Figs. 12e and 12f) in various proportions of VIN and PCP-CL show only the major water signal at $\delta = 4.02$, 4.05, or 4.11 ppm.

As a completion of this research, the *in vivo* bioavailability of the vinpocetine after oral administration in rats of the 1:4 and 1:10 wt coground systems and corresponding physical mixtures was assessed against a commercial vinpocetine oral formulation (Vimpocetin® 5 mg capsules, Pharma). In Figure 13, the plasma concentration profiles are presented, while the pharmacokinetic parameters are listed in Table 4.

Both physical mixtures, thanks to the presence of the hydrophilic polymer, showed a very little bioavailability enhancement with respect to the drug in the marketed formulation, but the very remarkable increase of drug bioavailability was achieved in the binary systems treated by mechanochemical activation. In particular, 1:4 and 1:10 wt coground systems resulted an oral relative bioavailability of 5.1 and 1.8 in comparison with Vimpocetin®, respectively. Furthermore, different from the commercial formulation having its t_{max} at 120 min, the plasma profiles of both coground systems revealed their C_{max} after only 30 min, testifying that this approach is a viable means to achieve an oral system with faster absorption times.

Contrary to the evidence of the *in vitro* performances, the highest oral bioavailability was obtained with the 1:4 wt coground system. This fact is quite interesting and testified that high amounts of crospovidone are not necessary in the formulation to promote an *in vivo* vinpocetine bioavailability enhancement. This means, a reduced drug dilution in the final formulation. Further it gives evidence that the process has a preponderant effect on the *in vivo* bioavailability.

A possible explanation of the behavior of the 1:10 wt can be found by checking the particle size of the

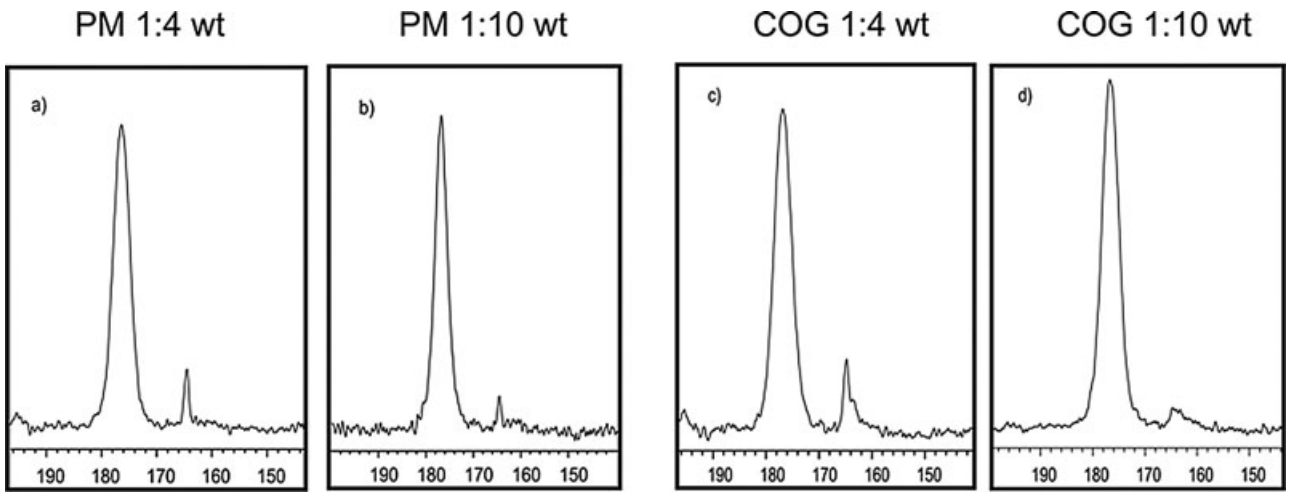

Figure 11. Carbonyl region of ^{13}C CP/MAS NMR spectra of 1:4 wt physical mixture (a), 1:10 wt physical mixture (b), 1:4 wt coground mixture (c) and 1:10 wt coground mixture (d).

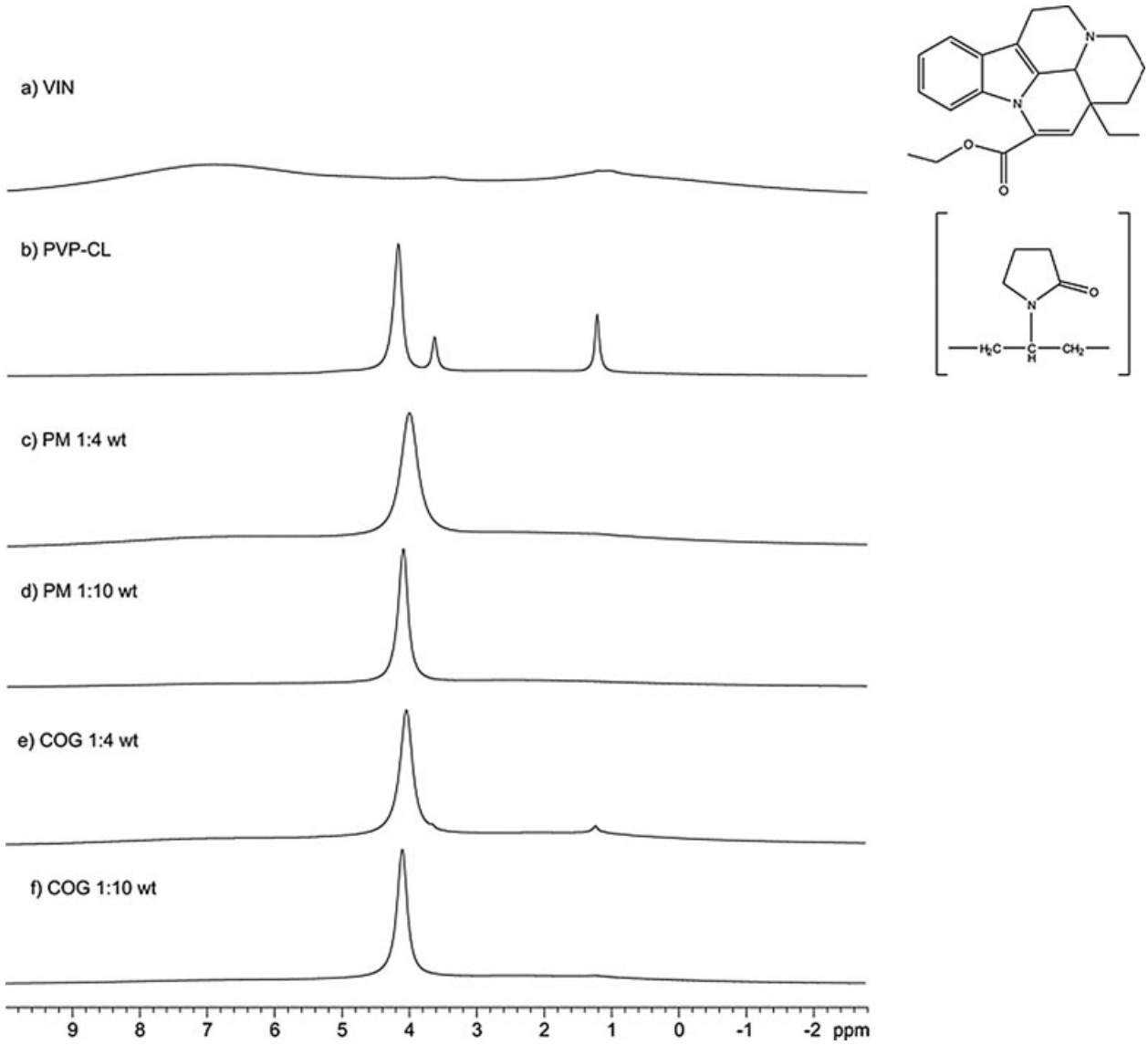

Figure 12. ^{1}H MAS NMR spectra of a) VIN, b) polymer PVP-CL, c) physical mixture 1:4 wt, d) physical mixture 1:10 wt, e) coground mixture 1:4 wt and f) coground mixture 1:10 wt

coground particles. In Figure 14, the particle volume percentage as a function of the diameter in a log scale of the 1:4 wt system coground for 180 min is depicted and compared with the 1:10 wt system coground for 180 min. It can be noticed that both samples showed a monomodal distribution, with a peak frequency value of 3.9 μm ($d_{0.5,}$ modal size fraction) in the case of 1:4 wt coground (Fig. 14a), and of about 15.6 μm for 1:10 wt coground (Fig. 14b). Furthermore, while 1:4 systems exhibited a narrow bell-shaped distribution with most particles ranging from 1.1 to 15 μm ($d_{0.1}$ to $d_{0.9}$), 1:10 composite distribution is very wide and ranged from 3.3 to 77.9 μm. This data confirm that increasing the amount of polymer, the particle size raised remarkably and the distribution became significantly wider. Hence, also in this case, in accordance with previous mechanochemical experiences with crospovidone,[20,34] the presence of large amount of this polymer can be responsible for the undesired formation of agglomerates, especially with the longest milling times. The presence of crospovidone, which contains 5% water content at the time of manufacture,[33] may cause the formation of large agglomerates, with a phenomenon probably similar to a wet granulation process.

These different dimensions of the coground samples can give reason for the differences in the *in vivo* performances. A possible explanation is hence that the larger agglomerates found in the coground containing large amounts of PVP-CL are responsible for the unexpected reduced *in vivo* performance.

Moreover, the unexpected lesser bioavailability of the 1:10 wt coground can be due to biological and hydrodynamic conditions—the little volume (2 mL) administered to the animals is probably not enough

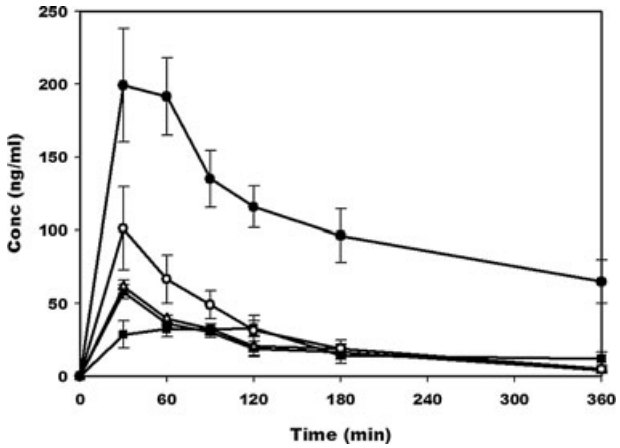

Figure 13. Mean plasma levels (±S.D.) of vinpocetine obtained after single oral dose (11 mg/kg): in 1:4 wt coground system (●), in 1:10 wt coground system (○), in 1:4 wt PM (▲), in 1:10 wt PM (△) and in commercial sample (Vimpocetin® 5mg)(■).

to efficiently disperse the entire dose in a 1:10 weight ratio with the polymer. Conversely, the 1:4 wt sample, having less amount of powder can be dispersed, and thus absorbed easier.

Another possible explanation is the presence of a thin stagnant layer originated by PVP-CL particle aggregation and adhesion on the intestine wall. In particular, in previous investigations,[35] clusters between intestinal mucus and ground polymeric particles were noticed. In this case, the difference in the thickness of stagnant layer, layer viscosity, and the interaction inside these clusters due to different amounts of crospovidone can explain the different absorption across the intestine membrane, and thus the different plasma profiles.

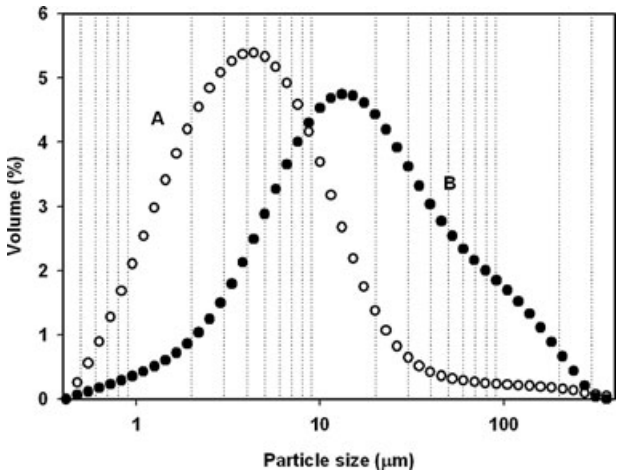

Figure 14. Particle size distribution of 1:4 (○, A) and 1:10 (●, B) drug-to-polymer wt ratio coground.

Aging Studies

The drug solid state in the selected coground samples (1:4 and 1:10 wt) was studied by repeating the DSC analyses every 4 months for a period of 1 year (data not shown). These curves are completely superimposable to that of freshly prepared samples, attesting the stability of the activated status (completely amorphous in the 1:10 wt and partially nanocrystalline in the case of 1:4 wt). Once embedded in the polymeric network, as clearly visible in TEM images reported in Figure 6a, the drug is stabilized in the metastable amorphous or nanocrystalline form. It is reasonable that the recrystallization is prevented by restricting drug mobility, thanks to the aforementioned interactions with the polymeric carrier and/or to the antiplasticizing effect of the polymer, that increases the viscosity of the binary systems and thereby decreases the diffusion of drug molecules necessary to form the lattice.[36] In the case of PVP-CL, the stabilizing potential has been reported in several cogrinding experiences.[20,37] The stability of the nanocrystalline/amorphous state of the drug is further facilitated by the energetic contribution of the mechanochemical activation.

CONCLUSION

Vinpocetine was successfully coground in a planetary mill, which made possible an enhancement of bioavailability through a solid-state activation. The effect of the amount of crospovidone and the milling time on vinpocetine activation in coground mixtures was statistically investigated. The drug release rate resulted directly related to the amount of polymer and milling time. In fact, as these variables increased, the drug was progressively transformed into an amorphous and/or nanocrystalline state extremely favorable for the *in vitro* dissolution. A multidisciplinary approach employed in the study of the sample permitted an extensive characterization of the changes induced on the drug solid state after mechanochemical activation. These analyses revealed the perturbation of the VIN carbonyl environment as a result of the disruption of the crystalline lattice, the absence of hydrogen bonding between components and the insurgence of hydrophobic interaction between crospovidone and VIN. Further the characterizations confirmed that the activated drug solid state was homogeneously present in the coground systems and was stable for at least one year.

A comparison with an oral commercial formulation (Vimpocetin®) revealed that the coground could enhance the oral bioavailability to fivefolds.

It can be concluded that the solid-state mechanochemical process in presence of micronized crospovidone is a viable means to improve the oral

bioavailability of vinpocetine through its transformation into a highly soluble-readily absorbable form.

ACKNOWLEDGMENTS

The authors thank Fondazione CRTrieste for funding, Linnea (Locarno, CH) for kindly donating the active ingredient used in this study, Prof. Francesco Princivalle for kind hospitality in the Deptartment of Earth Sciences, University of Trieste, and Lorenzo Magarotto for helpful discussions about solid state of the samples.

REFERENCES

1. Lorincz C, Szasz K, Kisfaludy L. 1976. The synthesis of ethyl apovincaminate. Arzneim-Forsch Drug Res 26:1907–1908.
2. Weinshaar RE, Bristol JA. 1990. In Comprehensive medicinal chemistry; Hansch C, Ed. Vol. II. Oxford, UK:Pergamon Press, pp 501–514.
3. Ribeiro L, Falcao AC, Patricio JAB, Ferreira DC, Veiga FJB. 2007. Cyclodextrin multicomponent complexation and controlled release delivery strategies to optimize the oral bioavalaibility of vinpocetine. J Pharm Sci 96:2018–2028.
4. Csanda E, Harcos P, Bacsy Z, Berghammer R, Kenez J. 1988. Ten years of experience with Cavinton. Drug Dev Res 14:185–187.
5. Szatmari SZ, Whitehouse PJ. 2003.Vinpocetine for cognitive impairment and dementia. Cochrane Database Syst Rev 1:CD003119
6. Grandt R, Beitinger R, Schateltenbrand R, Braun W. 1989. Vinpocetine pharmacokinetics in elderly subjects. Arzneimittel-Forschung 39:1599–1602.
7. Szakacs T, Veres Z, Vereczkey L. 2001. In vitro-in vivo correlation of the pharmacokinetics of vinpocetine. Pol J Pharmacol 53:623–628.
8. Kata M, Lukacs M. 1986. Enhancement of solubility of vinpocetine base with γ-cyclodextrin. Pharmazie 41:151–152.
9. Chen Y, Li G, Wu X, Chen Z, Hang J, Qin B, Chen S, Wang R. 2008.Self-microemulsifying drug delivery system (SMEDDS) of vinpocetine: Formulation development and in vivo assessment. Biol Pharm Bull 31:118–125.
10. Iosio T, Voinovich D, Grassi M, Pinto J.F, Perissutti B, Zacchigna M, Quintavalle U, Serdoz F. 2008. Bi-layered self-emulsifying pellets prepared by co-extrusion and spheronization: Influence of formulation variables and preliminary study on the *in vivo* absorption. Eur J Pharm Biopharm 69:686–697.
11. Cui S-X, Nie S-F, Li L, Wang C-G, Pan W-S, Sun J-P. 2009. Preparation and evaluation of self-microemulsifying drug delivery system containing vinpocetine. Drug Dev Ind Pharm 35(5): 603–611.
12. Kata M, Selmeczi B. 1987. Increasing the solubility of drugs through cyclodextrin complexation. J Incl Phen 5:39–43.
13. Kata M, Kedvessy G. 1987. Increasing the solubility characteristics of pharmaca with cyclodextrins. Pharm Ind 49(1):98–100.
14. Ribeiro L, Veiga F. 2002. Complexation of vinpocetine with cyclodextrins in the presence or absence of polymers. Binary and ternary complexes preparation and characterization. J Incl Phenom 44:251–256.
15. Ribeiro L, Loftsson T, Ferreira D, Veiga F. 2003a. Investigation and physicochemical characterization of vinpocetine-sulfobutyl ether β-cyclodextrin binary and ternary complexes. Chem Pharm Bull 51:914–922.
16. Ribeiro L, Ferreira D, Veiga F. 2003b. Physicochemical investigation of the effects of water-soluble polymers on vinpocetine complexation with b-cyclodextrin and its sulfobutyl ether derivative in solution and solid state. Eur J Pharm Sci 20:253–266.
17. Ribeiro L, Ferreira DC, Veiga FJB. 2005a. In vitro controlled release of vinpocetine-cyclodextrin-tartaric acid multicomponent complexes from HPMC swellable tablets. J Control Rel 103:325–339.
18. Ribeiro L, Carvalho RA, Ferreira DC, Veiga FJB. 2005b. Multicomponent complex formation between vinpocetine, cyclodextrins, tartaric acid and water-soluble polymers monitored by NMR and solubility studies Eur J Pharm Sci 24:1–13.
19. Ribeiro L, Carvalho RA, Ferreira DC, Veiga FJB. 2007. In vitro and *in vivo* studies on the complexes of vinpocetine with hydroxypropyl-β-cyclodextrin. Archiv Pharm Res 30:991–1001.
20. Voinovich D, Perissutti B, Magarotto L, Ceschia D, Guiotto P, Bilia AR. 2009a. Solid state mechanochemical simultaneous activation of the constituents of the Silybum marianum phytocomplex with crosslinked polymers. J Pharm Sci 98:215–228.
21. Voinovich D, Perissutti B, Grassi M, Passerini N, Bigotto A. 2009b. Solid state mechanochemical activation of Silybum marianum dry extract with betacyclodextrins: Characterization and bioavailability of the coground systems. J Pharm Sci 98:4119–4129.
22. Mathieu D, Nony J, Phan-Tan-Luu R. NEMRODW (new efficient technology for research using optimal design) software, LPRAI, Marseille , 1999.
23. R Development Core Team. 2009. R: A language and environment for statistical computing. R Foundation for Statistical Computing, Wien, Austria. ISBN 3-900051- 07-0. URL/http://www.R-project.org
24. Coceani N, Magarotto L, Ceschia D, Colombo I, Grassi M. 2010. Melting temperature, enthalpy and solubility dependence on crystal radius. The case of co-ground Nimesulide. J Phys Chem C (submitted).
25. Brun M, Lallemand A, Quinson JF, Eyraud C. 1973. Changement d'etat liquide-solide dans les milieux poreux. II Etude theorique de la solidification d'un condensat capillaire. J Chim Phys 70:979–989.
26. Zhang M, Efremov MY, Schiettekatte F, Olson EA, Kwan AT, Lai SL, Wisleder T, Greene JE, Allen LH. 2000. Size dependent melting point depression of nanostructures: Nanocalorimetric measurements. Phys Rev B 62:10548–10557.
27. Beleites C, Sergo V. 2009. http://hyperspec.r-forge.r-project.org for R (see reference 23)
28. Cadelli G, Zarattini P, Stebel M. 2007. Further refinements of tail artery cannulation in conscious rats, Centro Coordinamento e Sviluppo progetti e Apparecchiature (CSPA). Settore stabulario e sperimentazione animale. Università di Trieste, FELASA-ICLAS Joint Meeting 2007 –Villa Erba, Cernobbio (Co).
29. Vlase L, Bodiu B, Leucuta SE. 2005. Pharmacokinetics and comparative bioavailability of two vinpocetine tablet formulations in healthy volunteers by using the metabolite apovincaminic acid as pharmacokinetic parameter. **Arzneimittel-Forschung** 55:664–668.
30. Faraway JJ. 2004. Linear models with R (Chapman & Hall/CRC Texts in Statistical Science). vol. 63. Taylor & Francis , Boca Raton, FL, 188.
31. Magarotto L, Bertini S, Cosentino C, Torri G. 2001. Characterisation of nimesulide/b– cyclodextrin composite obtained by solid state activation. Mater Sci Forum 360-362:643–648.

32. Taylor LS, Zografi G. 1997. Spectroscopic characterization of interactions between PVP and indomethacin in amorphous molecular dispersions. Pharm Res 14:1691–1698.
33. Rawlinson CF, Williams CA, Timmins P, Grimsey I. 2007. Polymer-mediated disruption of drug crystallinity. Int J Pharm 336:42–48.
34. Grassi M, Coceani N, Magarotto L, Ceschia D. 2003. Effect of milling time on release kinetics from co-grounded drug-polymer systems. Proceedings of the AAPS Annual Meeting and Exposition, October, Salt Lake City, Utah.
35. Meriani F, Coceani N, Sirotti C, Voinovich D, Grassi M. 2004. In Vitro Nimesulide Absorption from Different Formulations. **J Pharm Sci** 93:3540–3552.
36. Van den Mooter G, Wuyts M, Blaton N, Busson R, Grobet P, Augustijns P, Kinget R. 2000. Physical stabilisation of amorphous ketoconazole in solid dispersions with polyvinylpyrrolidone K25. Eur J Pharm Sci 12:261–269.
37. Shin SC, Oh IJ, Lee YB, Choi HK, Cho CW. 1998. Enhanced dissolution of furosemide by coprecipitating or cogrinding with crospovidone. Int J Pharm 175:17–24.